Low Phonon Energy, Nd:LaF_3 Channel Waveguide Lasers Fabricated by Molecular Beam Epitaxy

T. Bhutta, A. M. Chardon, and D. P. Shepherd

Optoelectronics Research Centre

University of Southampton

Southampton SO17 1BJ, UK

E. Daran, C. Serrano and A. Muñoz-Yagüe

Laboratoire d'Analyse et d'Architecture des Systèmes du CNRS

31077 Toulouse Cedex 4, France

Abstract

We report the first fabrication and laser operation of channel waveguides based on LaF_3 planar thin films grown by molecular beam epitaxy. To our knowledge this is the lowest phonon energy dielectric material to have shown guided-wave laser operation to date. A full characterisation, in terms of spectroscopy, laser results and propagation losses, is given for the planar thin films upon which the channel waveguides are based. Two channel fabrication methods are then described, the first involves ion milling and the second takes the novel approach of using a photo-definable polymer overlay. Laser operation in Nd-doped samples is demonstrated at 1.06μm, 1.05μm and 1.3μm, and the potential for mid-infra-red laser sources based on such guides is discussed.

I INTRODUCTION

Fluoride crystals and glasses have many characteristics that make them attractive for use as rare-earth-doped laser hosts. In particular, they have lower phonon energies than oxides leading to the possibility of both mid-infrared (mid-IR) [1] and upconversion [2] lasers. Incorporating the fluoride host in an optical waveguide geometry can also offer low thresholds and high efficiencies, increasing the potential for continuous wave (cw) operation at room temperature and at relatively high power levels. This has been demonstrated most effectively with ZBLAN optical fibres [3-5].

The work described here is based on planar dielectric waveguides and with particular emphasis on the possibility of mid-IR operation. Planar devices are geometrically well suited to high-power diode pumping [6] and also hold the potential for the production of on-chip integrated devices. However, demonstrations of laser action in fluoride dielectric planar geometries have so far been quite limited, with only recent reports of near-IR (~1.06μm) lasing in Nd:YLF grown by liquid-phase-epitaxy [7] and Nd-doped fluoroaluminate glass by spin-coating [8]. Molecular beam epitaxial (MBE) growth of rare-earth-doped fluorides has been studied by several groups around the world [9-11]. Rare-earth-doped ZnF_2, PbF_2, CaF_2, and LaF_3 have all been grown with various substrate materials, including GaAs and Si. Recently, we demonstrated the first laser action in such an MBE-grown fluoride planar thin-film, based on Nd-doped LaF_3 [12]. The Raman spectrum of the LaF_3 waveguides shows a maximum phonon energy of just $380cm^{-1}$, in good agreement with reported values for bulk crystals [13]. This corresponds to the lowest phonon energy of any dielectric

waveguide laser reported to date. In comparison, ZBLAN fibres have a maximum phonon energy of 520cm^{-1} and GLS, another glass of interest for mid-IR laser sources, has a value of 425cm^{-1} [14]. The multiphonon relaxation quantum efficiency of LaF_3, previously investigated in Er- and Ho-doped bulk crystals [13,15], indicates that the cut-off for efficient radiative transitions is near 4μm. Consequently, the combination of this low phonon energy material with a low-loss guided geometry holds considerable potential for low threshold mid-IR lasers with output wavelengths comparable to, or beyond, those achieved by ZBLAN fibres.

In this paper we describe two methods for fabricating channel waveguides based on the MBE-grown LaF_3 thin films. The channel geometry is required to give the lowest lasing thresholds and can also give a more circular spatial output. For this first demonstration and investigation of such techniques, we have concentrated on Nd-doped films lasing at 1.06μm, as these are relatively easy to operate and characterise. The remainder of this paper is laid out as follows. Section II describes the fabrication of the planar thin films by MBE and their characterisation in terms of absorption and fluorescence spectroscopy, laser operation and optical loss. In section III we describe the fabrication of the slab-loaded channel waveguides by two different methods. Firstly, ion milling is used on a CaF_2-clad LaF_3 thin film in order to leave thin stripes of the cladding material to define the channels. Secondly, a photo-definable polymer overlay is used to make thin stripes on an unclad LaF_3 thin film, again to produce channel waveguides. The propagation modes of the channels are also discussed, both at the laser wavelengths investigated here and at mid-IR wavelengths. This is followed, in section IV, by an investigation of the laser characteristics of both types of channels, with a view to assessing the propagation losses. Finally, in section V, we

give our concluding remarks and discuss the prospects for mid-IR sources based on this technology.

SECTION II THIN FILM FABRICATION AND CHARACTERISATION

MBE is widely used for the fabrication of semiconductor devices, but there are few reports on the epitaxial growth of fluorides, especially on dielectric substrates. Nevertheless, this technique has been shown to allow creation of fluoride heterostructures with accurate control of thickness and composition [16]. This type of control can be useful to realize active waveguide components as it allows both refractive index and active layer engineering. Moreover, the thermodynamical conditions imposed during MBE growth (low temperature and growth rate) can favourably modify the incorporation of rare-earth ions compared to bulk crystals. For example, in the case of Er-doped CaF_2, MBE growth has been shown to allow a significant increase in the optically active doping level [17]. Fluorides are good candidates for MBE growth as the free energies of fluoride-molecule dissociation are exceptionally high, which means that the film will have the correct stoechiometry, even at low growth temperature, unlike oxides, which are transported in the vapour as dissociated species.

The MBE chamber used for these experiments is equipped with eight Knudsen effusion cells. For the thin films presented here, three cells were used loaded with CaF_2 crystal, LaF_3 crystal pieces, and NdF_3 compacted powder, respectively. The use of separate cells for the host matrix and the doping element allows the concentration

of the dopant to be easily controlled by changing the doping beam flux. The different effusion cells are calibrated separately by measuring the deposited layer thickness as a function of the cell temperature. This calibration is used to control the thickness as well as the composition of the different layers constituting the final structure. The Nd-doped-LaF_3 thin films studied in this paper were grown under ultra-high-vacuum conditions using (111) oriented CaF_2 substrates. Prior to the insertion of substrates into the chamber the CaF_2 surfaces are degreased using hot trichloroethylene and acetone, and then rinsed with deionised water. The substrates were mounted on a molybdenum block by indium soldering and a preheating process, under vacuum at a temperature above 600°C, was employed to obtain an oxygen-free surface. After this process, a CaF_2 buffer layer was grown on the substrate.

(111) oriented CaF_2 substrates have been chosen as this surface shows a hexagonal geometrical arrangement of the ions that should be the most suitable for the growth of the tysonite structure of LaF_3. Nevertheless, the lattice parameter mismatch between the Z = 2 cell of the hexagonal basal plane of LaF_3 (a = 4.148 Å) and the hexagonal symmetry unit of the CaF_2 (111) surface (a = 3.864 Å) is about 7%. The strain due to the parameter mismatch should be relaxed during the growth as the thickness obtained is large compared to the critical thickness and the growth temperature is 520°C. Consequently, the thin films were found to be free of cracks and exhibited a featureless surface under Nomarsky optical microscopy. Moreover, the dilatation coefficient difference at the interface CaF_2/LaF_3 is very weak compared to the case of fluoride/semiconductor heteroepitaxy ($\alpha(CaF_2) = 19.10^{-6}\ K^{-1}$, $\alpha(LaF_3) = 17.10^{-6}\ K^{-1}$, α (Si) = $2.5\ 10^{-6}\ K^{-1}$, α (GaAs) = $5.8\ 10^{-6}\ K^{-1}$), and no crystallographic defects due to this thermal mismatch have been observed.

The layers under study were grown at a substrate temperature of 520°C and at a growth rate of 0.6μm/hr. These conditions allow the growth of monocrystalline CaF_2 and LaF_3 films as confirmed by in-situ reflection high energy diffraction (RHEED) patterns. The Nd doping level was chosen to be 1% at., corresponding to LaF_3 and NdF_3 cell temperatures of 1165°C and 993°C respectively. In previous work we have reported high-resolution excitation spectroscopy, emission spectroscopy and lifetime measurements on hetero- and homoepitaxial layers in order to determine the influence of the substrate on the crystal quality and the influence of the Nd doping level on spectroscopic properties [18]. It was found that the highest luminescence intensity is obtained in the samples doped with 1 at.% Nd. For this concentration, the linewidth of the emission line around 1040nm at 10K for the films grown on CaF_2 is 0.6nm and for the films grown on LaF_3 substrates it is 0.3nm, whereas for the bulk material it is 0.2nm. So a broadening of the lines by about a factor 3 is observed in the heteroepitaxial films which is not due to the MBE growth process itself as this broadening is not observed for homoepitaxial thin films. It is well known for heteroepitaxial structures that the mismatch of the lattice parameters and the difference in the thermal expansion coefficients between the substrate and the layer can induce some residual stress which should produce some crystalline defects, reducing the homogeneity of the sample and broadening the emission lines of the Nd^{3+} ions.

In this work, we have carried out polarized absorption and emission spectroscopy of 1at.% Nd doped LaF_3 thin films at room temperature, in order to calculate the absorption and emission cross sections. The absorption spectroscopy was carried out using a tungsten lamp white light source. The light was coupled into

the waveguide using a large numerical aperture lens and the output was imaged with a microscope objective, via a polariser, into a Princeton Applied Research digital triple grating spectrograph with a silicon CCD detector array. The resulting polarized absorption spectra, corrected for the response of the system, are shown in figure 1. The calibrated spectra allow the calculation of the absorption cross sections at 788nm and 860 nm, the zones of interest for the AlGaAs and GaInAs diode pumping, with the results given in table 1.

A Judd-Ofelt analysis was then performed in order to calculate the cross sections of the emissions from the $^4F_{3/2}$ level [19,20]. The electric dipole line strengths $S^{ed}(J,J')$ for the transitions shown in figure 1 were calculated using

$$\int_{band} \alpha(\lambda) d\lambda = \frac{N 8\pi^3 e^2 \bar{\lambda}}{3hc(2J+1)} \frac{(n^2+2)^2}{9n} S^{ed}(J,J') \qquad (1)$$

where α is the absorption coefficient at wavelength λ, $\bar{\lambda}$ is the mean wavelength associated with the transition, n is the index of refraction at the mean wavelength, (2J+1) is the number of levels in the ground multiplet and N is the rare-earth-ion concentration. The Judd-Ofelt parameters, Ω_2, Ω_4, Ω_6, were then determined by fitting the calculated line strengths to the relation

$$S^{ed}_{JJ'} = \sum_{t=2,4,6} \Omega_t \left| \langle 4F^n(S,L)J | U^{(t)} | 4F^n(S',L')J' \rangle \right|^2 \qquad (2)$$

Values of reduced matrix elements $U^{(t)}$ were taken from Carnall [21]. The calculated Judd-Ofelt parameters are shown in table 2, and a good agreement is found with previously reported data for bulk Nd:LaF_3 crystals [22]. From the Judd-Ofelt

parameters, the line strengths were calculated for all the $^4F_{3/2}$ transitions using equation 2 and the appropriate matrix elements, and the inter-manifold spontaneous emission rates $A_{JJ'}$ were determined from

$$A_{JJ'} = \frac{64\pi^4 e^2 n}{3h(2J+1)\bar{\lambda}^3} \frac{(n^2+2)^2}{9} S^{ed}_{JJ'} \qquad (3)$$

The branching ratios, $\beta_{JJ'} = A_{JJ'} \Big/ \sum_{J'} A_{JJ'}$, were then calculated from these values and are given in table 3. The branching ratios were also determined experimentally by measuring the ratio of the 1.06μm to 1.35μm luminescence band intensities [23]. This ratio is used to determine the Ω_4/Ω_6 factor which allows calculation of all branching ratios. The results are in good agreement with the values calculated using Judd-Ofelt theory. From the emission rates, the radiative lifetime of the $^4F_{3/2}$ level can be calculated to be between 520μs and 650μs.

In figure 2 we present polarised emission spectra at room temperature from the $^4F_{3/2}$ level for a 1at.% Nd:LaF_3 thin film grown on a (111) oriented CaF_2 substrate. Three transitions are studied : $^4F_{3/2} - {}^4I_{9/2}$ around 900nm, $^4F_{3/2}$ - $^4I_{11/2}$ around 1050nm and $^4F_{3/2} - {}^4I_{13/2}$ around 1320nm. The spectra were obtained by pumping the sample with a Ti:sapphire laser at 790nm and recording the luminescence using an optical spectrum analyser, and correcting for the response of the system. Figure 3 shows the polarized effective stimulated emission cross section of the same sample for the $^4F_{3/2} - {}^4I_{11/2}$ and $^4F_{3/2} - {}^4I_{13/2}$ transitions. This was calculated from the fluorescence spectra using the relation [24,25]

$$\sigma_e^p(\lambda) = \frac{3\beta\lambda^5 I^p(\lambda)}{8\pi n^2 c \tau_{rad} \int \lambda \left[2I^\sigma(\lambda) + I^\pi(\lambda)\right] d\lambda} \qquad (4)$$

where τ_{rad} is the radiative lifetime of the upper manifold, $^4F_{3/2}$, and the superscript p denotes polarization s (TE) or p (TM). The values used for the branching ratios are given in table 3 and the radiative lifetime was taken to be 550μs. The calculated emission cross section for the 1.06μm band shown in figure 3(a) agrees well with that obtained for bulk Nd:LaF_3 [26], with a peak value of $2.7 \times 10^{-24} m^2$ for the π polarisation. The largest peak in the 1.3μm band is also π polarised and has a value of $3.2 \times 10^{-25} m^2$.

The laser performance of the planar thin films was tested using a resonator formed by butting two plane dielectric mirrors to the polished end faces of a waveguide consisting of a 3.6μm-thick Nd:LaF_3 thin film grown on a CaF_2 substrate with a 0.5μm CaF_2 cladding layer. The experimental procedure is that described in section IV, where the device was pumped using a Ti-Sapphire laser tuned to the peak Nd:LaF_3 absorption at 0.79 μm. It was found that the thin films gave TM polarised laser emission at 1.064 μm as would be expected from the fluorescence spectra. Using two highly reflecting mirrors (R > 99 % at 1.06 μm) a minimum absorbed pump-power threshold of 85 mW was achieved. By changing the output mirror to one with a transmission of 23% (at the laser wavelength), the threshold rose to 103 mW and with this output coupling we obtained a laser output power of 28 mW (for the available 440 mW of absorbed pump power) and a slope efficiency of 11 %. These results were the subject of a previous publication, and the reader is referred to Daran *et al* [12] for further details. The variation of the laser threshold with different

output couplers can be used to estimate the optical losses of lasers by the Findlay-Clay method [27]. For our planar thin film this gave a value for the losses at 1.064μm of 1.2 dB/cm [12]. The Findlay-Clay method and some of the potential problems associated with using it for our waveguides is discussed in more detail later in this paper (section IV).

SECTION III CHANNEL WAVEGUIDE FABRICATION

Channel waveguide structures have a number of advantages over their thin film counterparts that make them attractive sources for low power applications. The additional lateral confinement of both the pump and laser modes means that lower threshold devices are possible while, if additional propagation losses can be kept low, good slope efficiencies can be maintained. The channel geometry also provides a more circular spatial output, making them more compatible for low-loss coupling to fibre optic components. In addition, both passive and active channels can be integrated with other components on a single planar substrate using photolithographic techniques to produce integrated optoelectronic circuits.

We report on initial steps in developing channel technology based on MBE LaF_3 thin films. The work described here, concentrates on slab-loaded channels produced by fabricating a strip layer, of lower refractive index, over the light guiding core. This type of channel structure provides lateral confinement of the laser and pump modes because the effective refractive index experienced by the guided light is higher in the regions underneath the strip layer than in the adjacent planar areas which

have an air cladding (figure 4(a)). It also has the advantage that no modification of the active thin film is required (as opposed to techniques such as ion implantation or indiffusion). We report two methods of fabricating slab-loaded structures on MBE thin films; the first is via etching using a neutral argon ion-beam, the second is a novel method for producing slab loaded channel lasers using an organic photo-definable polymer, Benzocyclobutene (BCB).

Neutral ion beam etching (or physical sputtering) is a versatile and accurate micro-structuring technique that has been successfully employed on a wide variety of materials [28] and has been demonstrated to be suitable for producing low-loss channel waveguide lasers on other films [29]. The attractive feature of ion beam etching is that a high degree of control can be achieved. The ion energy, ion current density, etch angle and background pressure can all be varied independently to obtain optimum results, meaning that the etch quality is usually limited by the patterned photoresist mask (used to define the structure to be etched into the target), rather than the etching process itself.

The MBE planar film used to produce the ion-milled channels originally consisted of a 3.6 μm Nd:LaF_3 active core with a 0.3 μm CaF_2 protective cladding, on a CaF_2 substrate. The patterned photo-resist mask was prepared on this film using Micropost S1828 photo-resist to produce a 3 μm thick resist layer. For our first attempt at producing ion-milled channels on LaF_3 thin films we used a neutralised Argon-ion beam with a beam voltage of 500V and an ion current density of 0.45mA/cm^2, under a background pressure of 1.3×10^{-6} mbar. The sample was mounted on a rotating holder at an angle of 40° in an attempt to maximise the etch

rate. The sample was etched for 14 minutes, so that 0.4 μm of the exposed regions of the sample was removed. Although this degree of etching impinges onto the active layer, modelling of the channel waveguides based on the finite difference method, using a commercial modelling package from BBV Software and the index values in table 4, had shown that unless all the CaF_2 cladding was removed in the areas adjacent to the channels, the structures would offer reduced lateral confinement, especially for the smaller width channels. For example, for an 8μm width channel, etching 0.1μm into the core leads to a fundamental mode at 1.06μm that has all the power inside a width of 20μm, whereas leaving 0.1μm of cladding on the surface would give a width of 60μm. For this reason a 0.1μm safety margin was decided upon, and so the ion-milled structures can be thought of as a slab-loaded/rib hybrid (figure 4(b)).

We were successful in producing a number of structures of this form, with widths of 8, 11, 13, 17 and 20 μm, however we did encounter some post-fabrication problems. It was not possible to remove all the photoresist remnants from the top of some of the structures using either acetone or nitric acid (we could not use any abrasive methods due to the fragility of the sample). However, it is unlikely that these photoresist remnants significantly effect the operation of the device, as the scattering loss is not likely to be very high due to the negligible pump and laser mode intensities expected at the cladding-air interface. Figure 5 shows the calculated fundamental mode profiles at 800nm for the 8μm and 20μm channels (a) along with the experimentally observed output profiles (b). The latter were taken by imaging the waveguide throughput of a Ti:sapphire laser onto a CCD camera. While there is a good qualitative agreement, the waveguide can, in theory, support up to seven modes in the vertical dimension at this wavelength, and is single-moded for the 8μm channel

and double-moded for the 20μm channel in the horizontal dimension. Therefore the modal content of the experimental throughput is uncertain. Nevertheless, the images certainly show that we have obtained the channel waveguide confinement we were aiming for. These guides will also have five allowed modes in the vertical dimension at the lasing wavelengths investigated here. However, at the mid-IR wavelengths of interest in the long term, these guides are much nearer to being single mode while still giving good optical confinement. As an example figure 6 shows the calculated mode profile for the 8μm channel at a wavelength of 5μm, where only one mode is supported. Another positive point of our chosen waveguide structure is now apparent, in that the index difference between LaF_3 and CaF_2 is large enough to give good optical confinement into the mid-IR.

As an alternative approach to ion-milling we have also fabricated channel waveguides using BCB polymer overlays. The low-cost of polymer materials, combined with their versatility (in terms of waveguide geometry, material properties and architecture [33]) makes them very attractive for the fabrication of integrated optical components. Specifically, Benzocyclobutene (BCB) is an organic polymer with excellent planarisation, low moisture uptake, good adhesion and thermal stability [34]. Although BCB was originally developed as a thin-film dielectric coating for use in electronic multi-chip-modules [34], its low optical loss (0.8 dB/cm at 1.3 μm [35]) and refractive index of 1.5489 [32] (at 838nm), makes it suitable for combining with LaF_3 planar films to make channel waveguide structures. Moreover, BCB is available from DOW Chemical in a photosensitive form, which can be processed by using standard photolithographic techniques alone without the need for any etching. This greatly reduces both the time and cost of fabrication making it a more attractive

means for fabricating slab loaded structures (when compared to methods such as ion-beam milling) from both a commercial and practical point of view.

The MBE thin film used to produce the BCB channel waveguides originally consisted of an unclad 3.6 μm Nd:LaF_3 active layer on a CaF_2 substrate. The BCB can easily and quickly be applied to the active layer by spin coating. To achieve a 3.5 μm thick layer, the BCB was spun on to the MBE thin film at 4000 rpm for 30s, after an acceleration time of 30s, and was then pre-baked at 80°C for 95s in air to remove any residual solvents. The waveguides were patterned by placing the prepared sample in contact with a patterned chrome mask and exposing it to a UV lamp. After exposure, the sample was developed by immersing it in solvent to remove the unexposed regions of the BCB, leaving the channel structures. To complete the processing, the BCB was polymerised by curing it at 250°C for one hour in a tube furnace under nitrogen flow. The sample displayed well-defined channels and showed a smooth surface between these structures. The adherence of the BCB to the Nd:LaF_3 was sufficient to allow a standard end-polishing, resulting in waveguides of the form schematically shown in figure 4(c) and viewed through a microscope in figure 7. Modelling of these guides show that the strongest lateral confinement at 1.06μm is obtained for the 10μm and 5μm width strips, which both give a full mode width of around 10μm. Similarly to the ion-milled structures, these guides support many modes in the vertical dimension at 1.06μm, and range from single-moded to supporting up to 6 modes in the lateral dimension. In practice many of our results were taken using a 20μm width strip, as described in section IV, which could support up to 3 lateral modes. Figure 8 shows the theoretical fundamental guided mode spatial profile for this guide at 1.06μm.

SECTION IV CHANNEL WAVEGUIDE LASER PERFORMANCE

The lasing characteristics of the ion-milled and BCB channel waveguides were tested using the 1.064μm $^4F_{3/2} \rightarrow {}^4I_{11/2}$ transition of Nd:LaF_3, allowing an assessment of the propagation loss and general ease of use of these waveguides as lasers. Firstly, we investigated the ion-milled channels using a sample cut and end-polished to a length of 7.5 mm, so that the end-faces were perpendicular to the channels. Lightweight thin mirrors were directly butted to the end faces of the guide, in order to form the laser cavity, using a thin film of fluorinated liquid for adherence. Figure 9 shows the experimental apparatus used to test the laser performance. The Ti:sapphire pump laser was tuned to the strong Nd^{3+} absorption near 790nm with a polarisation corresponding to the TE modes of the waveguide and the σ polarisation of the LaF_3 crystal. TM polarised laser emission at 1.064μm was observed from the ion-milled channel structures with power thresholds, incident on the input mirror, as low as 26 mW. A range of output couplers, with different reflectivities (R) at the lasing wavelength, were butted to the waveguide and the threshold noted for each case. By plotting a graph of incident threshold power against –lnR we can estimate the propagation loss in the channel guide by the Findlay-Clay method [27]. The results of this analysis for the 8μm wide channel are shown in figure 10. The error bars give an indication of the variation in measured threshold values observed when re-butting the mirrors (approximately 10%). The intercept on the x-axis is related to the level of losses in the cavity, other than the output coupling, which we assume to be only due to propagation losses in the waveguide. The data for this channel suggests a propagation loss of 1dB/cm which is consistent with the value obtained for the planar thin film prior to ion beam milling [12].

However, observation of the lasing threshold for other channels on the same substrate showed considerable variations indicating a large variation in the quality of the channels obtained by our fabrication process. We also observed that the continued re-butting of mirrors quickly led to damage to the end-faces of the waveguide suggesting a very poor fragility of the milled structures. We believe this damage, combined with non-optimised launching optics (see later discussion of the BCB channels) led to the low observed output power of just 5mW when using a 23% output coupler and 300mW of incident power. Nevertheless, despite the non-optimised nature of the fabrication procedure and the use of launching optics not matched to the asymmetric mode profile of the channels, we have already obtained a large reduction (x5) in the incident power required to reach threshold compared to the thin film waveguide [12]. The results obtained for the 8μm channel also show that we have been able to introduce lateral confinement with negligible additional propagation loss.

The experimental set-up of figure 9 was then used to test the BCB channel waveguides which had been cut and end-polished to a length of 9.5mm. Once again a large variation in the quality of the channel guides was observed and so we decided to concentrate on a 20μm wide stripe channel, which gave relatively good performance. Firstly, we investigated how the launch efficiency varied between using a single launch objective to produce a roughly circular pump beam profile, as shown in figure 9, and then using a cylindrical-lens telescope before the launch objective to produce an asymmetric beam focus better matched to the expected mode profile of the waveguide. For the 20μm channel the calculated ratio of the mode width to height is

around 6.6 and using a telescope of similar magnification (f_1=125mm and f_2=19mm) we were able to increase the measured launch efficiency from 30% (with no telescope) to as high as 73%. From these results we can conclude that the ion-milled channels discussed previously are likely to have suffered from low launch efficiency as no effort was made to shape the pump beam in that case, even though the guided mode profile was similarly asymmetric. Using a final spherical focussing lens of focal length 10.8mm we obtained the laser results shown in figure 11 using a 23% output coupler. The efficiency of 14% with respect to absorbed power is very similar to that observed in the planar thin film using the same output coupling (11%) [12]. This again suggests that a negligible increase in propagation loss has been incurred due the additional fabrication steps required to achieve the lateral confinement, and that the losses are therefore around 1dB/cm. Indeed, achieving this slope efficiency, given the value of output coupling and the ratio of the pump and signal photon energies, suggests that the losses must be <2dB/cm. The lowest observed incident power threshold of 17mW for a 23% output coupler is 2.6 times lower in comparison to the ion-milled channels, but this is thought to be mainly due to the improved launching optics used in the case of the BCB channels. We were unable to carry out a Findley-Clay type analysis for these guides due to the fact that we again quickly observed end-face damage due to the re-butting of mirrors. Indeed, the fragility of both types of channel waveguide fabricated here is a major practical drawback and is an issue that requires further investigation. However, we have successfully fabricated channel waveguides by two different methods that have greatly improved the lasing threshold of the Nd:LaF_3 thin films, while maintaining reasonable output efficiency and not significantly increasing the thin film propagation loss. Future work must concentrate on lowering this background loss level, and on improving the robustness

of the channels, perhaps by using protective overlays. Occasionally laser operation on the 1.05μm line was also observed with the BCB channels. This line has a slightly lower emission cross-section than the 1.06μm line, which is normally observed, but with some output couplers the varying reflectivity of the mirrors was sufficient to allow such operation. Before end-face damage preceded too far we were also able to observe laser action at 1.3μm using two highly reflecting mirrors at this wavelength. However, this was using the non-optimised launching optics and so the observed incident power threshold of 250mW could certainly be improved upon.

SECTION V SUMMARY

We have characterised Nd:LaF_3 thin films grown by MBE on CaF_2 substrates, finding similar spectroscopic properties to bulk materials and waveguide losses of around 1dB/cm at 1.06μm. We have also successfully demonstrated two methods of fabricating slab-loaded channel waveguides based upon these low phonon energy thin films. The first method involves ion-milling of a CaF_2 overcladding and the second uses a photodefinable BCB overlay. Both methods led to channel guides whose laser characteristics are consistent with a negligible increase in propagation loss compared to the background level of the thin film. The ion-milled channels are suitable for producing strong optical confinement out to mid-IR wavelengths due to the relatively high index difference between CaF_2 and LaF_3, but the BCB based channels are likely to suffer from material absorption at these wavelengths. A major issue with both types of guide is the fragility of the end-faces. This was exaggerated in our experiments by our use of butted mirrors to form the monolithic laser cavity rather

than direct coatings, but is an issue that requires some action. The use of protective overlays, or the use of another fabrication technique, such as ion-indiffusion, which would allow the guide to be buried under a protective cladding layer will be considered. The combination of low-loss, high-optical confinement, and low phonon energies, together with the exceptional control of the MBE fabrication method and possibilities for integration, makes rare-earth-doped LaF_3 waveguides a very interesting candidate for mid-IR laser sources.

The authors wish to acknowledge Anne Tropper and Dan Hewak for useful discussions. This work is funded in part by an EPSRC grant (GR/N09787) and T. Bhutta acknowledges the support of an EPSRC studentship.

References

1. N.P.Barnes and R.E.Allen, "Room temperature Dy:YLF laser operation at 4.34μm", *IEEE J. Quantum Electron.*, vol.QE-27, pp. 277-282, 1991.
2. R.J.Thrash and L.F.Johnson, "Up-conversion laser-emission from Yb^{3+}-sensitized Tm^{3+} in BaY_2F_8", *J. Opt. Soc. Am. B*, vol.11, pp. 881-885, 1994.
3. R.Paschotta, N.Moore, W.A.Clarkson, A.C.Tropper, D.C.Hanna, and G.Maze, "230 mW of blue light from a thulium-doped upconversion fiber laser", *IEEE J. Sel. Top. Quant.*, vol.3, pp. 1100-1102, 1997.
4. B.Srinvasan, J.Tafoya, and R.K.Jain, "High-power 'Watt-level' cw operation of diode-pumped 2.7μm fiber lasers using efficient cross-relaxation and energy transfer mechanisms", *Opt. Express*, vol.4, pp.493-495, 1999.
5. J.Schneider, C.Carbonnier and U.B.Unrau, "Characterisation of a Ho^{3+}-doped fluoride fibre laser with a 3.9μm emission wavelength", *Appl. Opt.*, vol.36, pp. 8595-8600 , 1997.
6. C.L.Bonner, T.Bhutta, D.P.Shepherd, and A.C.Tropper, "Double-slad structures and proximity coupling for diode-bar-pumped planar waveguide lasers", *IEEE J. Quantum Electron.*, vol.QE-36, pp. 236-242, 2000.
7. P.Rogin and J.Hulliger, "Epitaxial Nd:YLF linear waveguide laser", *Opt. Lett.*, vol. 22, pp. 1701-1703, 1997.
8. D.W.J.Harwood, E.R.Taylor, C.T.A.Brown, D.P.Shepherd, and D.N.Payne, "Novel fabrication technique for the realisation of planar glass waveguides", presented at European Conference on Optical Communications, Madrid, Spain, paper WdA34, 1998.

9. L.E.Bausa, C.Fontaine, E.Daran, and A.Munoz-Yague, "Molecular beam epitaxy of Nd-doped CaF_2 and $CaSrF_2$ layers on Si and GaAs substrates", *J. Appl. Phys.*, vol.72, pp.499-503, 1992.

10. R.A.McFarlane, M.Lui, and D.Yap, "Rare earth doped fluoride waveguides fabricated using molecular beam epitaxy," *IEEE J. Sel. Top. Quant.*, vol.1, pp. 82-91, 1995.

11. J.M.Ko and T.Fukuda, "Molecular beam epitaxy of Ca1-xRxF2+x (R=Nd,Er) layers: study of RHEED pattern and lattice mismatch", *J. Cryst. Growth*, vol.200, pp. 490-497, 1999.

12. E.Daran, D.P.Shepherd, T.Bhutta, and C.Serrano, "Laser operation of Nd:LaF_3 thin film grown by molecular beam epitaxy", *Electron. Lett.*, vol. 35, pp. 398-400, 1999.

13. L.A.Riseberg and H.W.Moos, "Multiphonon orbit-lattice relaxation of excited states of rare-earth ions in crystals", *Phys. Rev.*, vol.174, pp. 429-438, 1968.

14. T.Schweizer, D.J.Brady, and D.W.Hewak "Fabrication and spectroscopy of erbium doped gallium lanthanum sulphide glass fibres for mid-infrared laser applications", *Opt. Express*, vol.1, pp.102-107 , 1997.

15. M.J.Weber, "Probabilities for radiative and non-radiative decay of Er^{3+} in LaF_3", *Phys. Rev.*, vol.157, pp. 262-272, 1967.

16. A.Yu.Khilko, S.V. Gastev, R.N.Kyutt, M.V.Zamoryanskaya, and N.S.Sokolov, "Structural and luminescence studies of CdF2-CaF2 superlattices on Si(111)", *Appl. Surf. Sci.* , vol.123-124, pp. 595-598, 1998

17. E.Daran, R.Legros, A. Muñoz-Yagüe, C.Fontaine, and L.E.Bausá, "1.54μm wavelength emission of highly Er-doped CaF2 layers grown by molecular beam epitaxy," *J. Appl. Phys.*, vol.76, pp. 270-273, 1994.

18. F.Lahoz, E.Daran, X.Zhang, A. Muñoz-Yagüe, R.Cases, and R.Alcala, "Hetero- and homoepitaxial Nd^{3+} doped LaF_3 thin films grown by molecular beam epitaxy: a spectroscopic study", *J. Appl. Phys.*, vol.86, pp. 3699-3704, 1999.

19. B.R. Judd, "Optical absorption intensities of rare-earth ions," *Phys. Rev.*, vol.127, pp750-761 1962.

20. G.S. Ofelt, "Intensities of crystal spectra of rare-earth ions," *J. Chem. Phys.*, vol.37, pp.511-520, 1962.

21. W.T.Carnall, P.R.Fields, and K.Rajnak, "Electronic energy levels in the trivalent lanthanide aquo ions. I. Pr^{3+}, Nd^{3+}, Pm^{3+}, Dy^{3+}, Ho^{3+}, Er^{3+}, Tm^{3+}," *J. Chem. Phys.*, vol.49, pp.4424-4442, 1968.

22. W.F.Krupke, "Optical absorption and fluorescence intensity in several rare-earth-doped Y_2O_3 and LaF_3 single crystals," *Phys. Rev.*, vol.145, pp. 325-337, 1966.

23. T.S.Lomheim, L.G. DeShazer, "Optical-absorption intensities of trivalent neodymium in the uniaxial crystal yttrium orthvanadate," *J. Appl. Phys.*, vol.49, pp. 5517-5522, 1978.

24. P.F.Moulton, "Spectroscopic and laser characteristics of Ti:Al_2O_3," *J. Opt. Soc. Am. B,* vol.3, pp.125-133, 1986.

25. B.F.Aull and H.P.Jensen, "Vibronic interactions in Nd:YAG resulting in nonrepricosity of absorption and stimulated-emission cross-sections," *IEEE J. Quant. Elect.,* vol.QE18, pp. 925-930, 1982.

26. T.Y.Fan and M.R.Korta, "End-pumped Nd:LaF_3 and Nd:$LaMgAl_{11}O_{19}$ lasers," *IEEE J. Quantum Electron.*, vol. QE-25, pp. 1845-1849, 1989.

27. D.Findlay and R.A.Clay, "The measurement of internal losses in a 4-level laser," *Phys. Lett.*, vol.20, pp.277-278, 1966.

28. PR Puckett, SL Michel, and WE Hughes "Ion beam etching" in *Thin Film Process II*, J.L.Vossen and W.Kern, Ed. Boston:Academic Press, 1991, pp.749-782.

29. R.Gerhardt, J.Kleine-Borger, L.Beilschmidt, M.Frommeyer, H.Dotsch, and B.Gather, "Efficient channel-waveguide laser in Nd:GGG at 1.062μm wavelength," *Appl. Phys. Lett.*, vol.**75**, pp.1210-1212, 1999.

30. E.D. Palik, *Handbook of optical constants of solids II.* Boston: Academic Press, 1991, p.832.

31. R.Laiho and M. Lakkisto, "Investigation of the refractive indices of LaF_3, CeF_3, PrF_3 and NdF_3", *Philisophical Magazine B*, vol.48, pp.203-207, 1983.

32. S.W.Guo, G.Gustafsson, O.J.Hagel, H.Arwin, "Determination of refractive index and thickness of thick transparent films by variable-angle spectroscopic ellipsometry: application to benzocyclobutene films", *Appl. Opt.*, vol.35, pp. 1693-1699, 1996.

33. L.Eldada and L.W.Shacklette, "Advances in polymer integrated optics", *IEEE J. Sel. Top. Quant.*, vol.6, pp. 54-68, 2000.

34. R.Foster, "Photoimagable BCB technology lowers costs for MCMs", *Solid State Technol.*, vol.38, pp. 125-130, 1995.

35. C.F.Kane and R.R.Krchnavek, "Benzocyclobutene optical waveguides", *Photon. Technol. Lett.*, vol.**7**, pp.535-537, 1995.

Table Captions

Table 1 Absorption cross-sections for 1at.% Nd:LaF_3 thin film.

Table 2 Judd-Ofelt parameters.

Table 3 Calculated radiative rates, and calculated and measured branching ratios, for a 1at.% Nd:LaF_3 thin film.

Table 4 Refractive index values. The values used are from the references quoted. If values were not available for the exact wavelength then an approximate value is used based on interpolation from nearby wavelengths.

Table 1

Wavelength (nm)	Absorption cross section ($10^{-24}m^2$)	
788	π	2.1 ± 0.1
	σ	1.6 ± 0.1
860	π	1.5 ± 0.1
	σ	0.75 ± 0.1

Table 2

	Nd:LaF_3 1at.% (this work)	Nd:LaF_3 5at.% [22]
Ω_2 / 10^{-20} cm^2	1.2 ± 0.2	0.35
Ω_4 / 10^{-20} cm^2	2.5 ± 0.4	2.57
Ω_6 / 10^{-20} cm^2	3.0 ± 0.5	2.50

Table 3

Transition	$A_{JJ'}$ (s^{-1})	$\beta_{JJ'}$ (calculated)	$\beta_{JJ'}$ (measured)
$^4F_{3/2} \rightarrow {}^4I_{9/2}$	730 ±130	40 ±1	38.4
$^4F_{3/2} \rightarrow {}^4I_{11/2}$	910 ± 140	50 ± 1	50.6
$^4F_{3/2} \rightarrow {}^4I_{13/2}$	180 ± 25	9.8 ± 0.2	10.50
$^4F_{3/2} \rightarrow {}^4I_{15/2}$	8.8 ± 1.5	0.5 ±0.02	0.5

Table 4

Wavelength / μm	CaF_2 [30]	LaF_3 (n_e) [31]	BCB [32]
0.79	1.43065	1.59189	1.5512
1.06	1.42856	1.58922	1.5448

Figure Captions

Figure 1 Absorption spectra of a 1at.% Nd:LaF_3 thin film for σ (a) and π (b) polarisation.

Figure 2 Polarised emission spectra at 300K for a 1at. % Nd:LaF_3 thin film. (line : π polarisation, dots : σ polarisation)

Figure 3 Polarized effective stimulated emission cross section at room temperature for (a) $^4F_{3/2} - ^4I_{11/2}$ and (b) $^4F_{3/2} - ^4I_{13/2}$. (line : π polarisation, dots : σ polarisation)

Figure 4 Channel waveguide geometries.

Figure 5 Calculated (a) and experimentally observed (b) mode profiles for the 8μm (upper) and 20μm (lower) ion-milled channel waveguides.

Figure 6 Calculated mode profile for the 8μm ion-milled waveguide at a wavelength of 5μm.

Figure 7 Microscope pictures of the polished end-face of the BCB channel waveguides of various widths.

Figure 8 Theoretical fundamental guided mode for the 20μm wide BCB slab loaded channel waveguide at 1.06μm.

Figure 9 Experimental arrangement for waveguide laser characterisation.

Figure 10 Plot of incident power threshold against –lnR for the 8μm wide ion-milled channel waveguide.

Figure 11 Output power against absorbed pump power for the 20μm wide BCB channel waveguide.

Figure 1

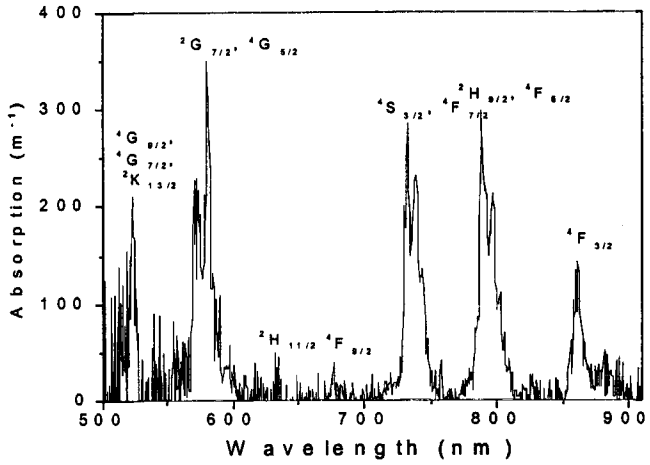
Absorption (m⁻¹)
Wavelength (nm)
0
100
200
300
400
500
600
700
800
900
$^2G_{7/2}$, $^4G_{5/2}$
$^4G_{9/2}$, $^4G_{7/2}$, $^2K_{13/2}$
$^4S_{3/2}$, $^4F_{7/2}$
$^2H_{9/2}$, $^4F_{5/2}$
$^4F_{3/2}$
$^2H_{11/2}$ $^4F_{9/2}$

(a)

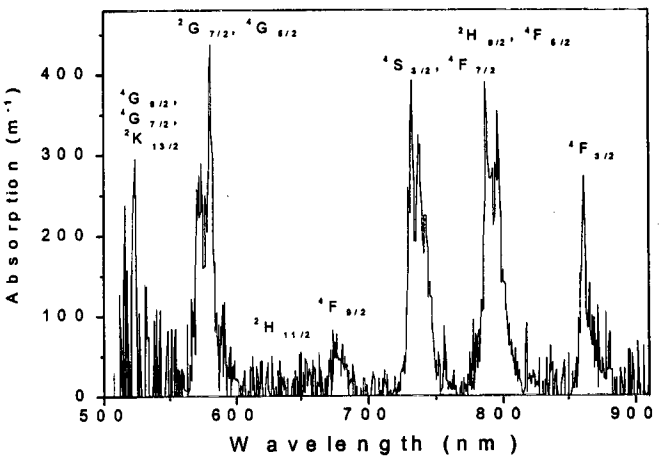
Absorption (m⁻¹)
Wavelength (nm)
0
100
200
300
400
500
600
700
800
900
$^2G_{7/2}$, $^4G_{5/2}$
$^4G_{9/2}$, $^4G_{7/2}$, $^2K_{13/2}$
$^4S_{3/2}$, $^4F_{7/2}$
$^2H_{9/2}$, $^4F_{5/2}$
$^4F_{3/2}$
$^2H_{11/2}$
$^4F_{9/2}$

(b)

Figure 2

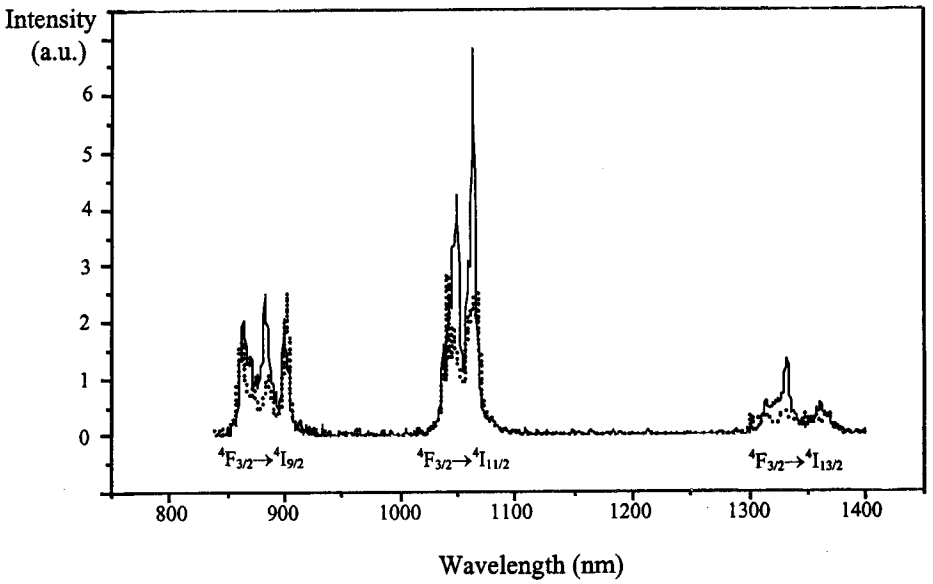
Intensity
(a.u.)
0
1
2
3
4
5
6
800
900
1000
1100
1200
1300
1400
Wavelength (nm)
$^4F_{3/2} \rightarrow {}^4I_{9/2}$
$^4F_{3/2} \rightarrow {}^4I_{11/2}$
$^4F_{3/2} \rightarrow {}^4I_{13/2}$

Figure 3

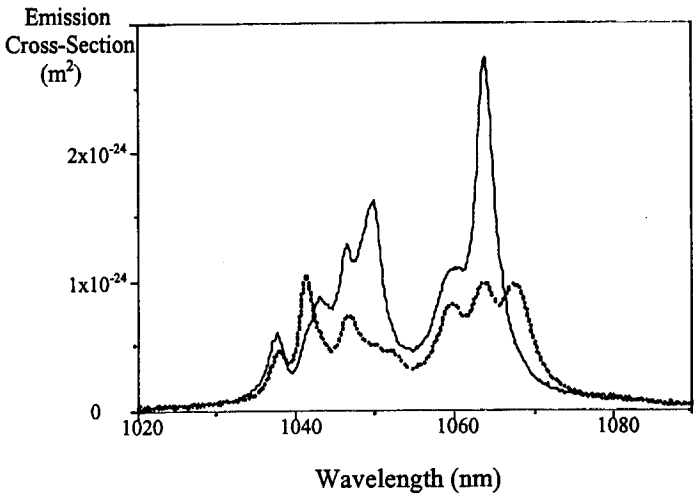
Emission
Cross-Section
(m²)
2x10⁻²⁴
1x10⁻²⁴
0
1020
1040
1060
1080
Wavelength (nm)

(a)

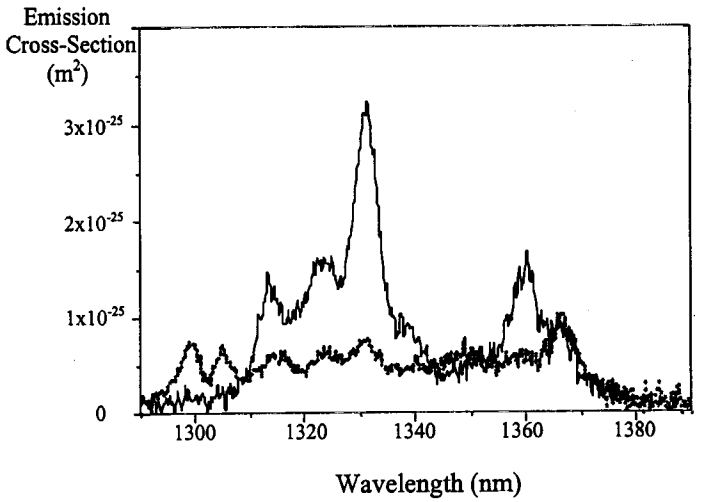
Emission
Cross-Section
(m²)
3x10⁻²⁵
2x10⁻²⁵
1x10⁻²⁵
0
1300
1320
1340
1360
1380
Wavelength (nm)

(b)

Figure 4

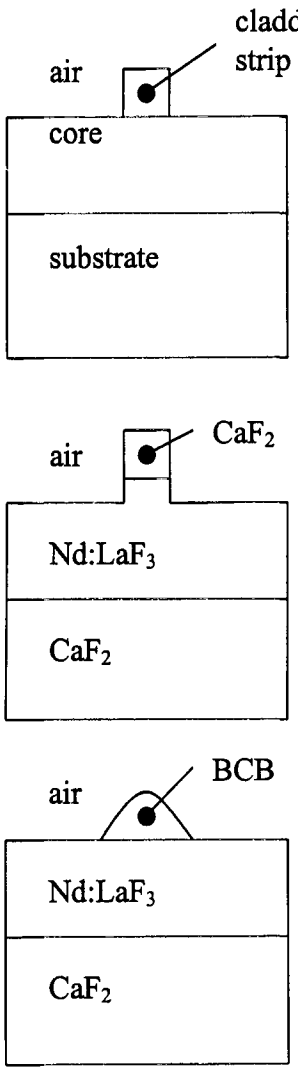

a) Standard Slab Loaded Geometry

b) Ion-Milled Channel Waveguide

c) Polymer Overlay Channel Waveguide

Figure 5

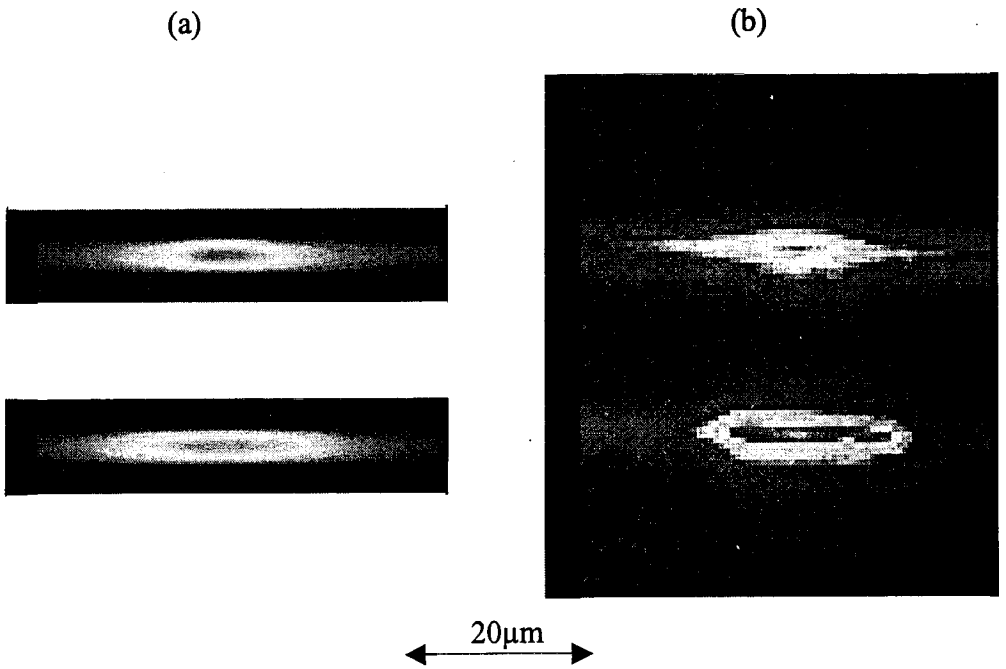

Figure 6

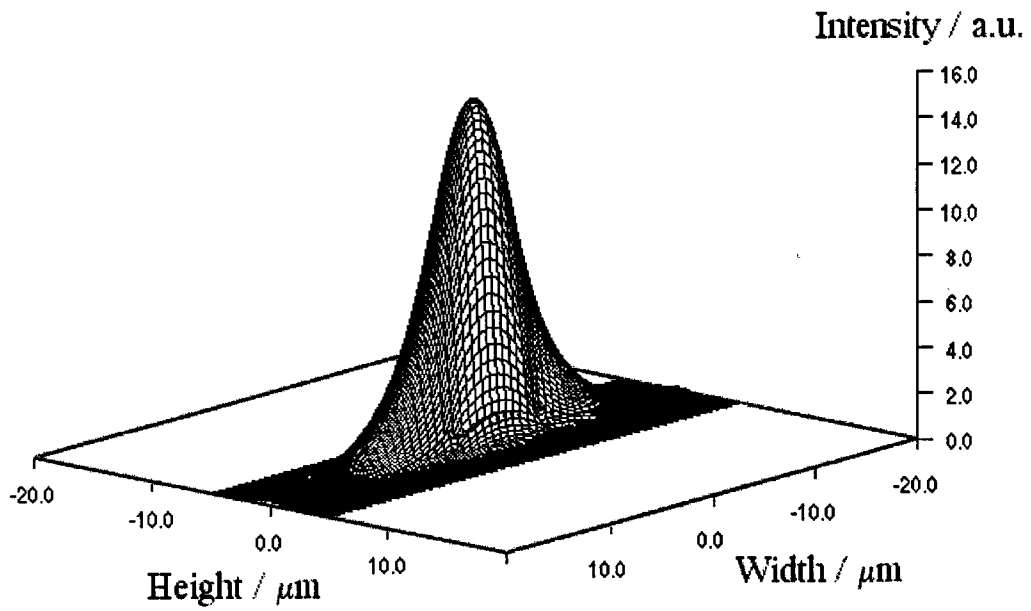
Intensity / a.u.
16.0
14.0
12.0
10.0
8.0
6.0
4.0
2.0
0.0
-20.0
-10.0
0.0
10.0
Height / μm
-20.0
-10.0
0.0
10.0
Width / μm

Figure 7

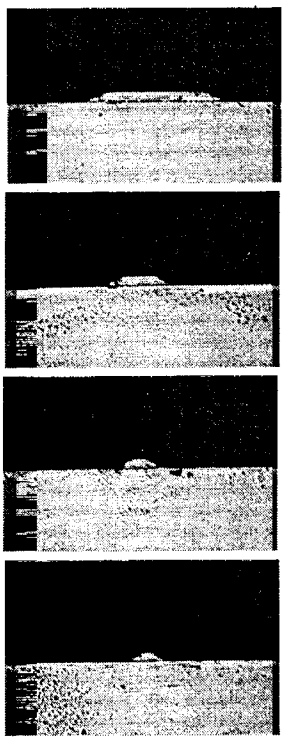

Figure 8

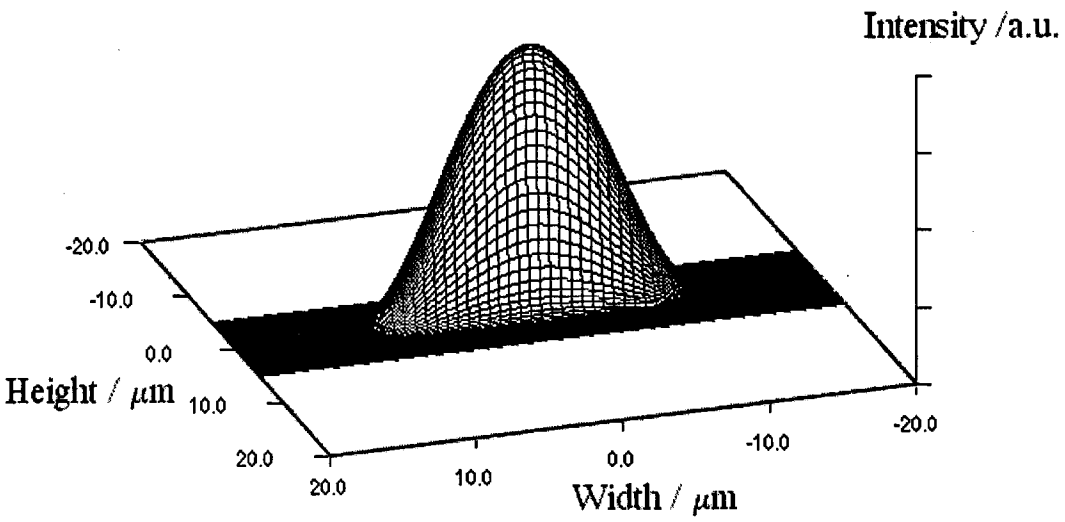
Intensity /a.u.
-20.0
-10.0
0.0
10.0
20.0
Height / μm
20.0
10.0
0.0
-10.0
-20.0
Width / μm

Figure 9

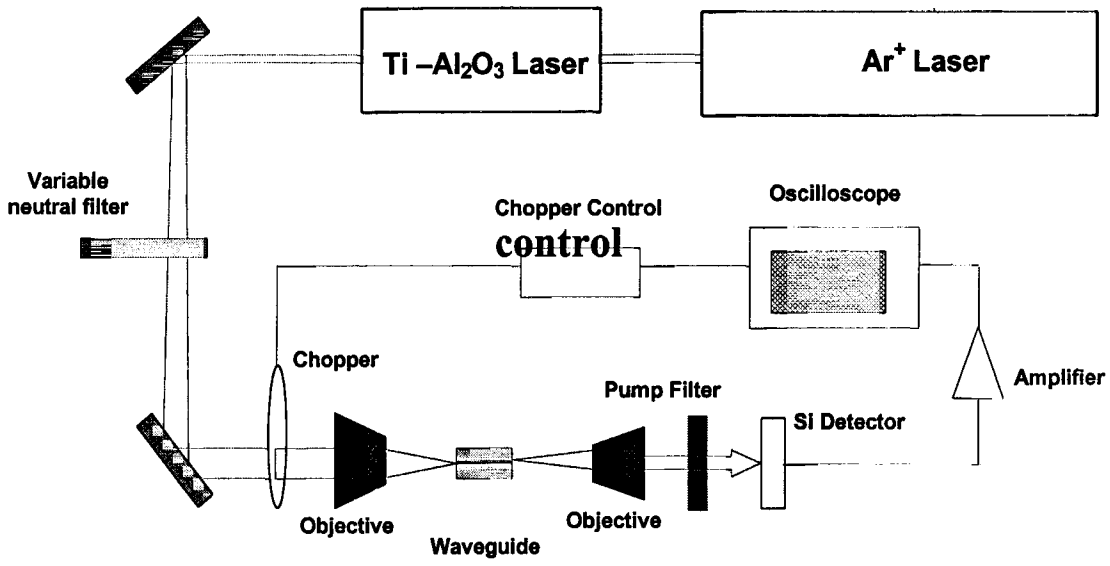
Ti –Al2O3 Laser
Ar+ Laser
Variable
neutral filter
Chopper Control
control
Oscilloscope
Chopper
Pump Filter
Si Detector
Amplifier
Objective
Waveguide
Objective

Figure 10

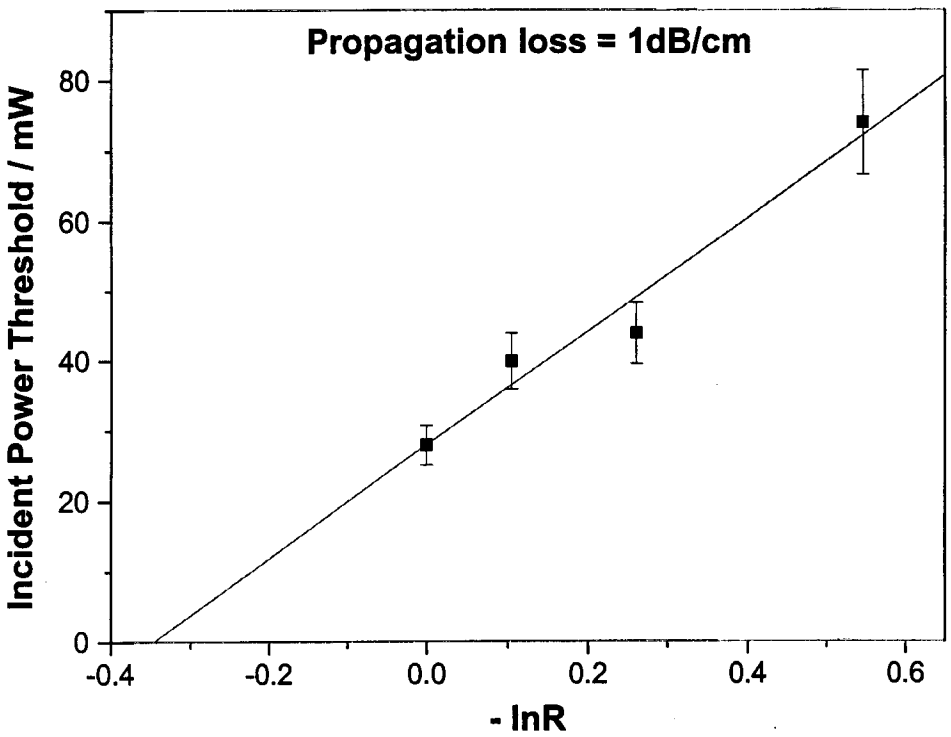
Propagation loss = 1dB/cm
Incident Power Threshold / mW
80
60
40
20
0
-0.4
-0.2
0.0
0.2
0.4
0.6
- lnR

Figure 11

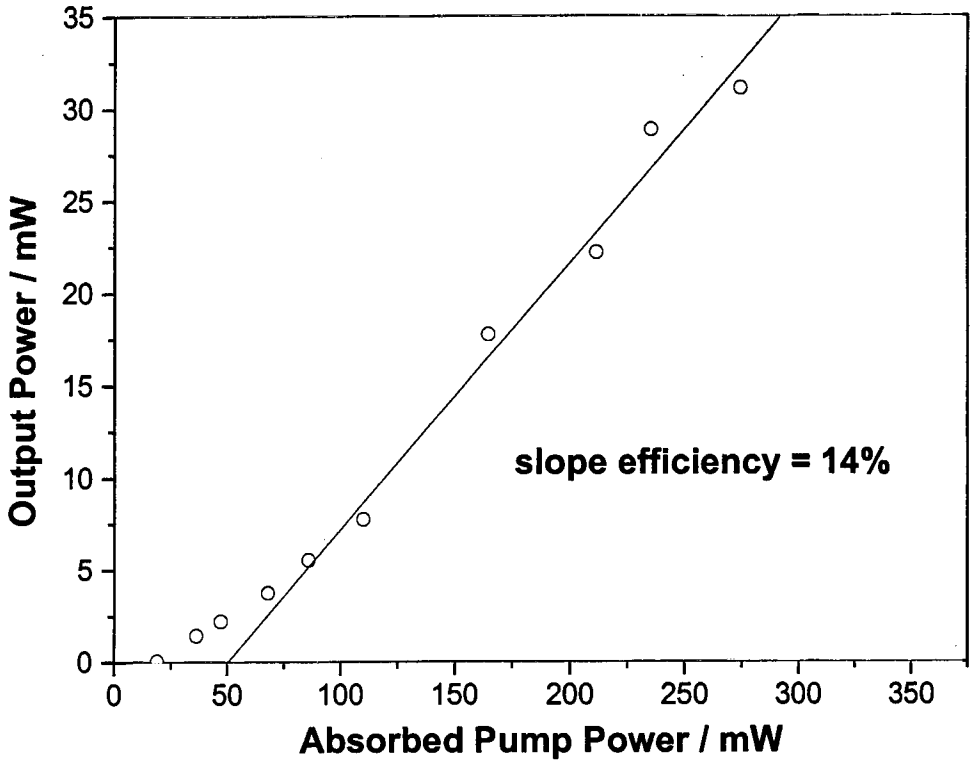
Output Power / mW
Absorbed Pump Power / mW
slope efficiency = 14%
0
5
10
15
20
25
30
35
0
50
100
150
200
250
300
350